



Geothermal signature of basaltic flows using aeromagnetic data, west Cairo area, Egypt

Haby S. Mohamed¹ · Mahmoud M. Senosy¹ · Heba Salah¹

Received: 4 November 2020 / Accepted: 1 May 2021 / Published online: 18 May 2021
© Saudi Society for Geosciences 2021

Abstract

Tertiary volcanics in Egypt are basaltic flows. These are recorded in the subsurface of Nile Delta and west Cairo in the Khattatba and Abu Roash regions but exposed on Gabal Qatrani. Such flows and structure trends made west Cairo the focus of geothermal exploration. The present study aimed to discover the geothermal resource and its relation with basaltic flows and subsurface structures in the area. To achieve these aims, aeromagnetic data (TMI) map, scale 1:500,000, was used. The source parameter imaging technique was used to calculate the depth of basement rocks. The results indicated that depth to the basement varies from 700 m at Khattatba and Abu-Roash regions to 4400 m southward and at G. Muqattam in the extreme eastern parts. These results are verified by subsurface data of three drilled deep wells. The detected major structure trends run in three directions: east-west, northeast-southwest, and northwest-southwest. The Curie point depth (CPD), geothermal gradient (GG), and heat flow (HF) were all calculated using the spectral analysis technique. CPD values range from 14 km in the eastern parts of the area to 34 km in the south-west. The GG values range from 15 to 33 °C/km. The HF values range between 38 and 86 mW/m². The high GG and HF values recorded at Khattatba and Abu-Roash are due to the basaltic flows in the subsurface. The two regions are considered reservoirs that were promising for geothermal energy. Increase in thickness of the sedimentary cover to 4000 m southward indicates the possibility of hydrocarbon occurrences.

Keywords Aeromagnetic data · Curie point depth · Geothermal resources

Introduction

Egypt was an exorogenic foreland during the Phanerozoic Era that experienced sedimentation, affected by intermittent event volcanicity. These volcanicitys and igneous activity occurred mainly concerning the fracture system, which originated in the late Precambrian. The periodical reactivation of these fracture zones throughout the Phanerozoic resulted in different plutonic and volcanic rock formation types. Various phases of igneous and volcanic rocks were formed during Paleozoic and Mesozoic, whereas the Cenozoic volcanism is largely basaltic (Said 1990; Baldrige et al. 1991).

The geothermal activities in Egypt are intimately related to more factors. The nature and intensity of magmatic activity and the nature of invaded rocks and tectonic activity in the area represented these factors (Hochstein 1990). The most pronounced effects of geothermal activities in Egypt were connected with the Tertiary volcanicity, which is common in the northern parts of Egypt in the form of basaltic flows. The Tertiary basaltic rocks, especially near Cairo at Abu Roash and north El-Fayum at Gabal Qatrani, were studied by different authors such as Bayoumi and Sabri (1971), Said (1981), and Williams and Small (1984). The basaltic rocks are found either in the form of dykes or lava flows. The lava flows are formed by the uprise of the subcrustal basaltic magma through fissures and faults that originated in the basement complex and re-activated in Oligocene and Miocene ages. Numerous studies have focused on geochemistry, petrography, magma type, tectonic environment, and the age of these volcanoes. On the other hand, information concerning the basaltic direction flow and depth to basement rocks was minimal. Abdel Monem and Heikal (1981) discussed the main element composition, tectonic environment, and magma type of the

Responsible Editor: Domenico M. Doronzo

✉ Haby S. Mohamed
habysalaheldin@aun.edu.eg

¹ Geology Department, Faculty of Science, Assiut University, Assiut 71516, Egypt

Mesozoic to Recent basalts in Egypt. They concluded that the Alkali olivine basaltic magma type for the volcanoes of Bahariya Oasis and the Nile district erupted on a continental crust. While the Quartz tholeiitic magma type for the Tertiary basalts of Gabal Qatrani, Gabal Abu Roash, Abu Zaabal, and the Cairo-Suez erupted on an oceanic crust. Amer et al. (1982) discussed the petrography and petrochemistry of the subsurface basalts of Abu Hammad wells and pointed out that these basalts are said to be oceanic tholeiites. Moghazi (2003) studied the geochemistry of the Tertiary continental basalt suite of the Red Sea coastal plain. Lucassen et al. (2008) explained the isotope composition of Late Mesozoic to Quaternary intraplate magmatism in northeastern Africa (Sudan, Egypt) and showed that the Nd, Pb, and Sr isotope signatures are surprisingly uniform in the mantle. Endress et al. (2011) studied the geochemistry of 24 Ma basalts from NE Egypt and indicated a polybaric fractionation history with initial crystallization at 12–18 km. Abu El-Rus and Rooney (2017) identified two types of intraplate basalt eruptions from the Tertiary volcanism in middle Egypt: (1) sub-alkaline hypersthene

normative basalts and (2) alkaline nepheline normative basalts. Abu El-Rus et al. (2018) studied a new bulk-rock and mineral analyses and radiogenic isotope data to select the most basic flows from the Natash volcanic field and showed that the lavas are mainly of alkaline affinity and have a continuous affinity. The composition spectrum ranges from alkali olivine basalt (AOB) to trachyte and rhyolite to all basaltic lavas in the province record different degrees of fractional crystallization of olivine, clinopyroxene, plagioclase, and spinel. However, some geophysical studies were applied to estimate the Curie depth from the spectral analysis of aeromagnetic data, such as Aboud et al. (2011), Saibi (2015 a,b), Dogan et al. (2017), Abdel Zaher et al. (2018), Elbarbary et al. (2018), Mohamed (2021), and Raj Kumar et al. (2021), but these studies did not focus on Tertiary basalts. Hence, the recent study was oriented to apply the aeromagnetic geophysical studies in evaluating the geothermal activity and its relation with basaltic rock distribution and the subsurface structural trends that may control the occurrences of basaltic rocks at the west Cairo, especially for the area which is located in the extreme north of Egypt between longitude 29° 30' to 30° 30' N and latitude 30° 00' to 31° 30' E (Fig. 1).

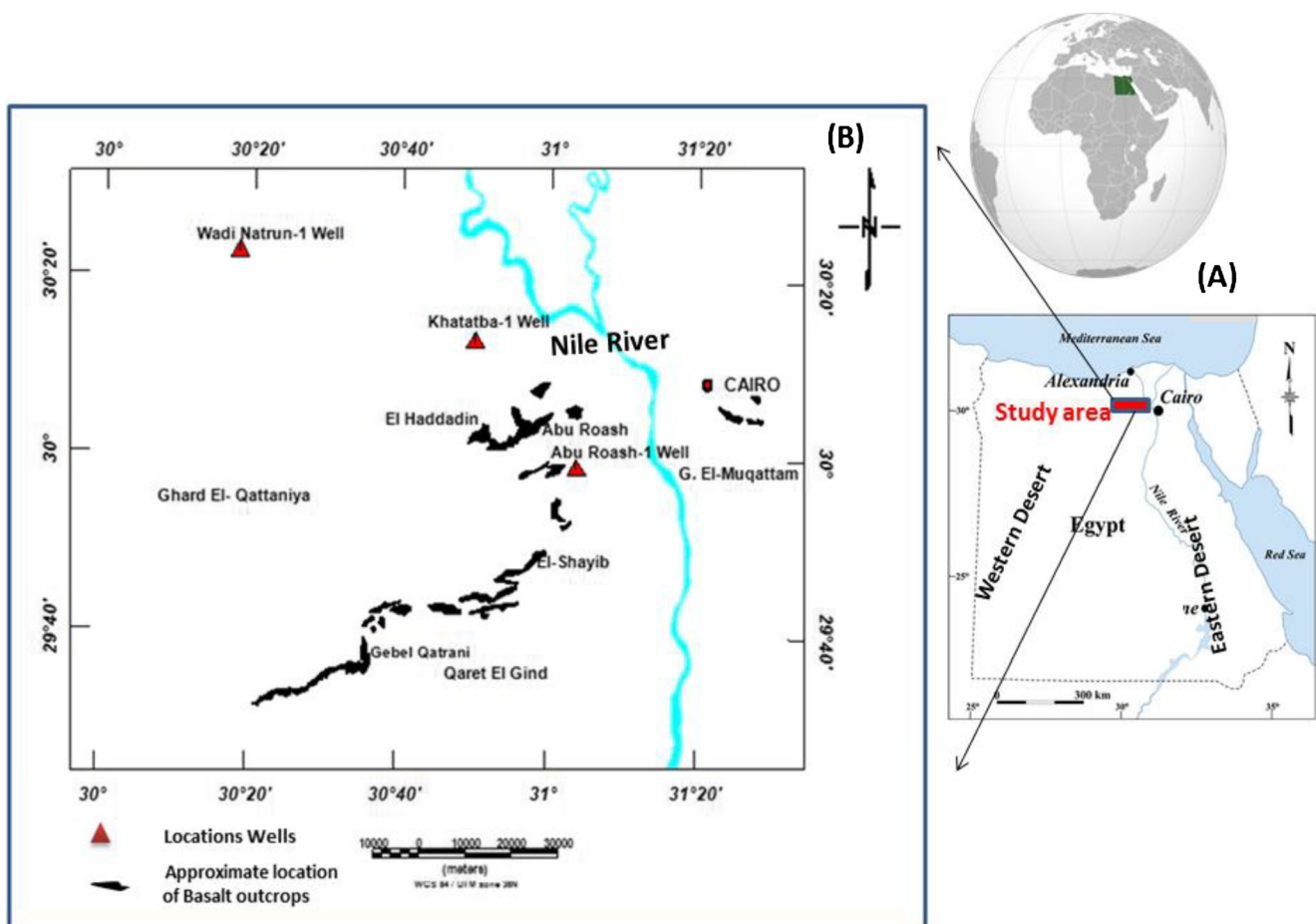


Fig. 1 A Map of Egypt showing the location of the study area in Fig. 1B

Geologic and structure setting

The study area’s lithostratigraphic units represent wide time span from Cretaceous to Quaternary (Fig. 2). These units are nominat-ed from base to top as Abu Roash Formation (Late Cenomanian–Santonian), Khoman Formation (Campanian–Maastrichtian), Mokattam Group (Middle Eocene), the Maadi group (Late Eocene), Gebel Qatrani Formation (Oligocene), Kashab Formation (Miocene), and Quaternary deposits.

The Khoman formation mainly consists of more than 50 m of fossiliferous, fractured chalky limestone (Norton 1967). Abu Roash Formation is classified into seven members arranged from top to base: ‘A, B, C, D, E, F, and G’ according to Aadland and Hassan (1972). The homogeneous calcareous limestone of the Khoman Formation contrasts with the embedded limestone and shale of the Abu Roash Formation; however, the contact between the two formations is covered by the progressive erosion of the soft lithology of unit ‘A.’ Mokattam Group (Giushi and Gebel Hof formation) belongs to the Middle Eocene and constitutes the foundation bedrock of the northern-eastern part of 15th of May City and its north-ern extension. The formation consists of white to yellowish-white, marly and chalky limestone, intercalated with a few interbeds of hard, dark, dolomitic limestone. The Giushi formation is a substantial section of thin-bedded and highly bio-turbated carbonates. Beds rich in Opercuurina pyamidum, serpulid, and bryozoan remain as a mark of this formation.

The Wadi Hof Formation is capped by highly fossiliferous sandy and dolomitic limestone beds.

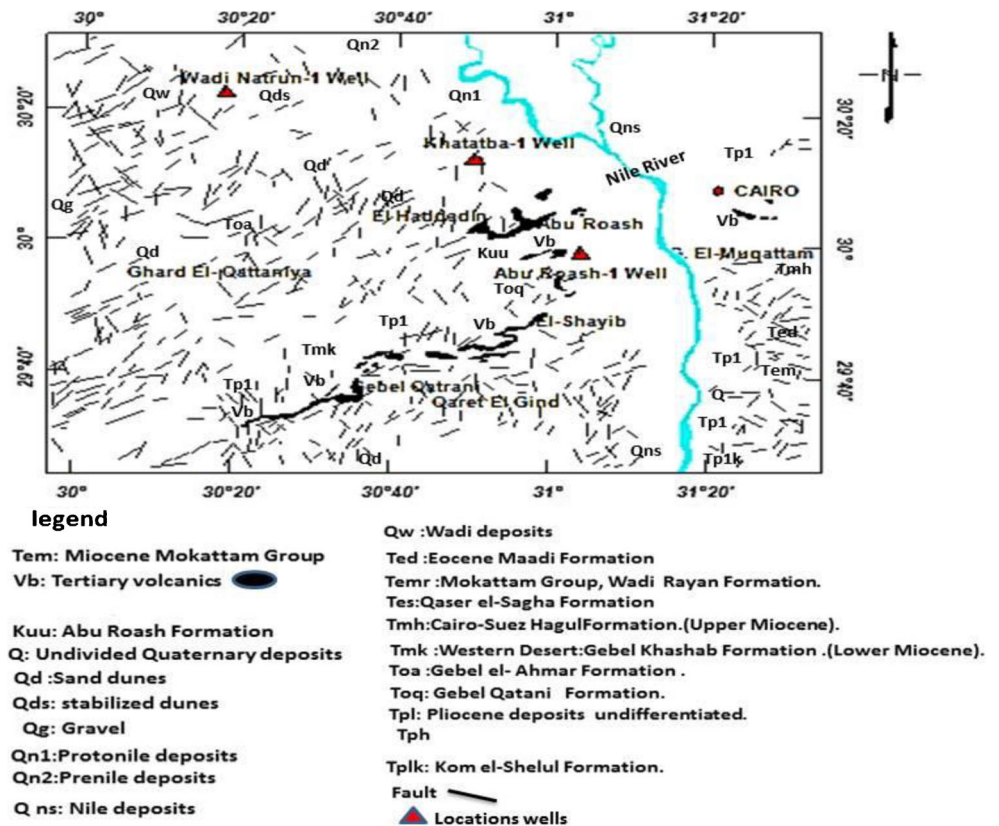
Maadi group (Late Eocene) sediments are more clastic than the underlying Mokattam sediments. Oligocene deposits over-lie the later deposits of the Eocene disconformably. They as-sume two distinct facies: a fluviatile facies of sand and gravels and open marine facies of shales and minor limestone inter-beds. The distribution of these sediments was mainly gov-erned by the volcanicity, geyser activity, and tectonism that affected the Red Sea regions and the belt of highs between the stable and unstable shelves during the Oligocene.

Gebel Qatrani Formation does not overlay the Widan El-faras Basalt (Bowen and Vondra 1974). This unconformity corresponds to the Rupelian–Chattian boundary (Gingerich 1992). Widan El-faras Basalt is overlain by the Miocene allu-vial Kashab Formation at the top of Gebel Qatrani. The con-tact is highly erosional, and the patches on top of basalt are sometimes filled with coarse sand and contain basalt debris and chert pebble conglomerate.

Quaternary deposits are spread all over Egypt and lay un-conformably over Pliocene or older rocks. These deposits are closely related to climatic changes and sea-level fluctuations during the Pleistocene period; their mode of origin groups them into Eolian, fluvial, and marine sediments.

Structurally, the study area is located within the Unstable Shelf in the northern parts of Egypt. This shelf is complex with frequent folds, fractures, and faults. Most

Fig. 2 Geological map showing the surface structures of the study area (after the Egyptian Geological Survey and Mining Authority, 1981)



faults, as mentioned by Refai et al. (1973), are trending NE, and the macrostructure described in the area is in the form of NE, and WNW en echelon folds dissected by NE, NW, and WNW normal faults, NE reverse, and thrust faults, and NE, NW, and WNW conjugate strike-slip faults (Fig. 2). These faults are complying with thermal springs and volcanic activity. In different parts of Egypt, Tertiary volcanoes found their way along these faults, especially in Abu Raosh and Gebel Qatrani, where several basalt outcrops occur. Rittmann (1954) and Salem (1976) believed that this volcanic activity in northern Egypt was related to renewed tension along African northwest-trending subcrustal lineaments. Swedan (1991) mentioned that the oldest rocks exposed in the Greater Cairo area occupy the anticlinal structure of Abu Raosh. Faults and folds mainly control the structural pattern of the Greater Cairo region.

Methodology and data acquisition

Available data

Aeromagnetic data at a mean terrain clearance of 1000 m in the form of a unified 1-km grid of total magnetic intensity (TMI) with 10-nT contour intervals and line spacing of 3000 m with a scale of 1:500,000 (Getech 1992; Green et al. 1992) were used. The data were obtained from the GETECH Group PIC. Also, the subsurface stratigraphic data of three deep wells drilled in the study area (Wadi Natrun-1, Abu Roash-1, and Khatatba-1 well) and that reached the basement surface at depths of 4042 m, 1795 m, and 1872 m, respectively, are used to verify the results.

Processing and interpretation of the aeromagnetic data

All processing and interpretation of the aeromagnetic data in the present study were completed by using Oasis Montaj Program (2014). The general magnetic field in the study area used in the processing was computed using a magnetic declination of 2.6° east and a magnetic field inclination of 43.57°. The resulted regional magnetic field intensity was 41,849 nT. These parameters were used to calculate the filter technique of aeromagnetic data. The TMI and RTP of the aeromagnetic data were interpreted qualitatively and quantitatively.

Qualitative interpretation of the aeromagnetic data

The qualitative interpretations of the aeromagnetic data included applying of title derivative filter (TDR) and tracing of the aeromagnetic lineaments that reflect the predominant subsurface structure lines in the study area. The aeromagnetic

lineaments were traced based on the concepts of Gay (1972). The major lineaments are considered deep-seated structures that originated in the basement and extended upward in the sedimentary cover. Along some of these lineaments, basaltic eruptions have occurred in addition to geothermal activity. The following is a brief description of both the TMI and RTP aeromagnetic maps as well as the corresponding tilt derivative maps.

The TMI of the study area (Fig. 3a) shows positive and negative magnetic anomalies. The magnitudes of these anomalies vary from -140 to +70 nT. The western part of the study area elongated to an oval positive anomaly with a magnitude of about +70 nT is observed. This anomaly is associated with Qattaniya uplift. Meanwhile, major negative anomalies with magnitudes -140 nT and -80 nT are present in the southern parts. These anomalies are corresponding to Gebel Qatrani and El Gindi basins.

The negative anomalies in the study area are accordant to the low magnetic susceptibility basalt observed by Abdel Monem and Heikal (1981), where the Egyptian Tertiary basalts appear to compete compositionally from nepheline to quartz normative. The Cairo-Suez district's basalts, Abu Zaabal and Abu Roash, which constitute the northern belt, are typically quartz-normative, and the basalts of Gebel Qatrani and Nile Valley are quartz-normative grading into olivine-normative. So, the type of basaltic rocks affects the observed magnetic field value and the effectiveness of weathering on the mineralogy and chemical composition of the basaltic rocks in the area. The area that includes basalt outcrops has the same magnetic anomaly (magnetic value is negative and varies from -125 to -25 nT). The source of the magnetism in this area could be the existence of one magma type underground and most likely the same origin and age.

Generally, the major magnetic anomaly pattern is aligned along with E-W and NE-SW directions. This pattern is reflecting the main structure lines in the study area. As the study area is located at latitudes 29° 30' to 30° 30' N that corresponds to an inclination of 43.57°, both positive and negative peaks of the magnetic anomalies are not directly pointing to the occurrences of the corresponding geologic features. Therefore, the Geomagnetic Reference Field (IGRF) was removed, and the total magnetic intensity data were reduced to the pole (RTP) and presented as a contour map (Fig. 3b). The RTP aeromagnetic map shows no definite dislocation between the peaks of both positive and negative magnetic anomalies observed on the TMI map. However, positive anomalies on the RTP map appear to be clear in the northern and south-eastern parts. Also, the magnitudes of most magnetic anomalies vary from -210 to +120 nT, with a remarkable increase than that at the same locations on the TMI map. Most anomalies extend in E-W and NE-SW directions.

A tilt derivative filter (TDR) was applied to the TMI data to locate contacts between different rock units that differentiated

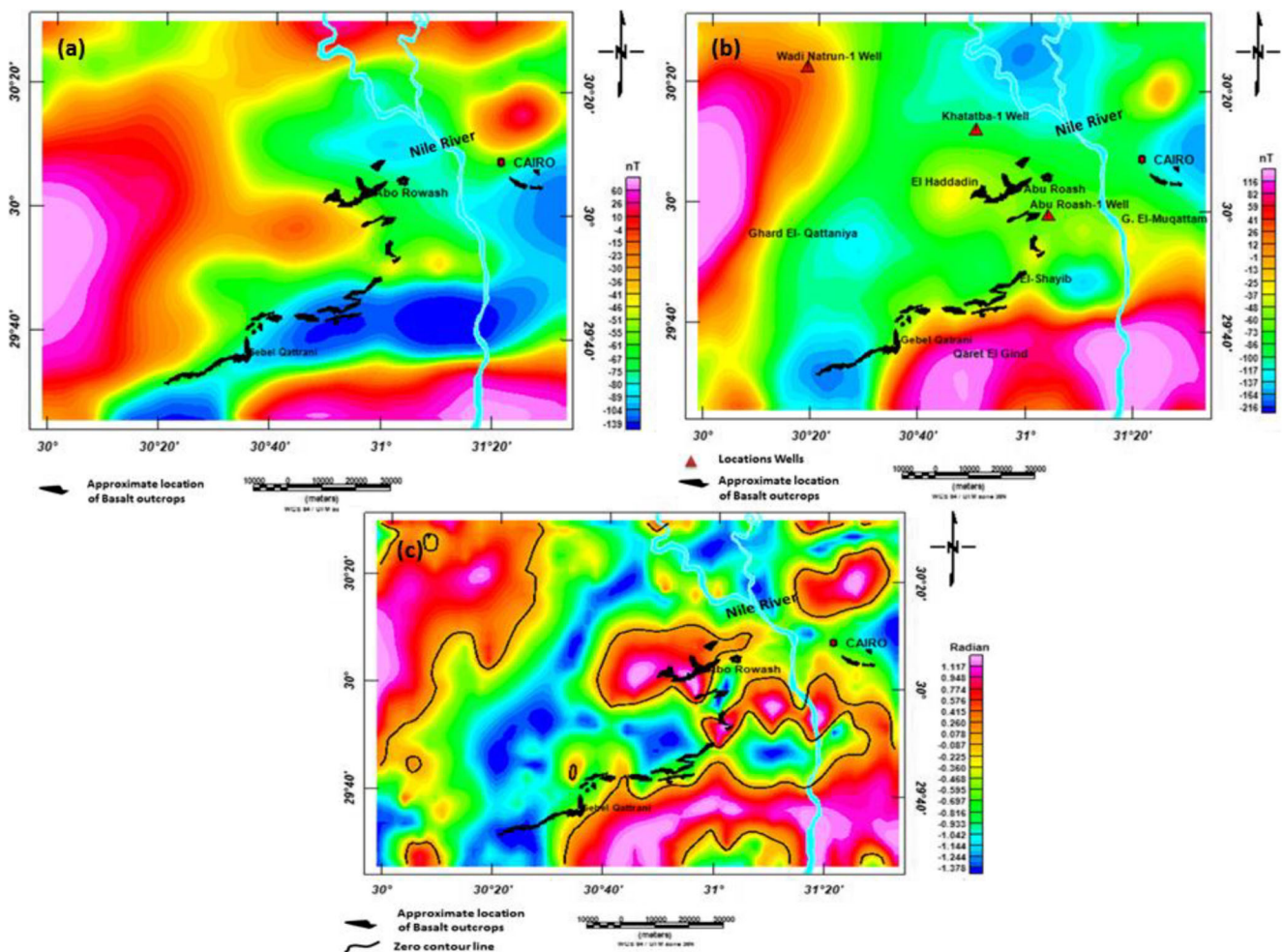


Fig. 3 a Total magnetic intensity (TMI) of the study area. b RTP aeromagnetic map of the study area. c Tilt derivative map of the study area; the black lines indicate the location of zero contour line

in magnetic susceptibility even if these contacts lithologically or structurally. The TDR was calculated from the ratio of the vertical derivative to the absolute value of the horizontal derivative (Verduzco et al. 2004). The TDR map (Fig. 3c) indicates that the major structural trends are in the magnitude of the tilt angle values, which range between -1.37 and 1.11 radians. According to Miller and Singh (1994), the positive values reveal anomalies over the source; meanwhile, the negative values are outside of the source location. Also, the zero contours are pointing to the source edges or structural lines. The E-W and NE-SW directions are the predominant trends in the study area. These directions are the main extensions of the basalt outcrops.

3.2.2. Quantitative interpretation of the aeromagnetic data

Spectral analysis (SA) and source parameter imaging (SPI) techniques were applied in the aeromagnetic data quantitative interpretation. The SA technique was applied to estimate the Curie point depth (CPD), geothermal gradient, and heat flow

in the study area; meanwhile, the SPI technique was used to estimate the basement depth and structural trends along which basaltic flows can erupt. The following is a summary of the applied technique and the results.

The source parameter imaging (SPI) function is one of the methods used to calculate the depth of basement rocks for estimating the source geometries, source dip, susceptibility, and density contrast (Thurston and Smith 1997; Kamba and Ahmed 2017). The source depth of the observed field and the local wavenumber (k), calculated for any point within a grid of data through horizontal and vertical gradients, were estimated using this method. Details of the source parameter imaging (SPI) technique and its applications are given in Nabighian (1972) and Thurston and Smith (1997).

In the present study, to confirm the accuracy of the SPI method, the subsurface stratigraphic data of three deep wells reach to surface basement rocks (Wadi Natrun-1, Abo Roash-1, and khatatba-1), were used as a control reference.

The Curie point depth (CPD): The occurrence of volcanic activity in the study area in the forms of dikes and sheets leads to a change in the basalt magnetization behaviour and the hosting

rocks; this is mainly resulting in converting magnetic minerals from ferromagnetic to paramagnetic at temperature $550 \text{ }^\circ\text{C} \pm 30 \text{ }^\circ\text{C}$ (Hsieh et al. 2014; Nwankwo and Shehu 2015). The depth to the Curie isotherm is defined as a theoretical surface with a temperature of $580 \text{ }^\circ\text{C}$ and Curie point depth (CPD) that is considered an index of the bottom of a magnetic source, due to the minerals of the Earth lose their ferromagnetic properties and fail to possess magnetization (Nur et al. 1999). The aeromagnetic anomalies can be used to study magnetic structures above the Curie point depth. Simultaneously, the geothermal gradient can be calculated from the temperature difference between the Earth's surface and Curie isotherm ($580 \text{ }^\circ\text{C}$) divided by the Curie point depth. The shallow Curie point depth (CPD) included the regions with geothermal potentials, such as the young volcanisms and areas of thin crust (Aydin and Oksum 2010). Knowing the varieties of the Curie depth in the area can provide important information on both regional and local temperature distribution, even there were no deep boreholes (Chapman and Furlong 1992; Ross et al. 2006; Komolafe 2010; Bansal et al. 2011, 2013).

Many authors published different methods for calculating CPD or the depth to the bottom of the magnetic layer (e.g. Spector and Grant 1970; Bhattacharyya and Leu 1975; Shuey et al. 1977; Okubo et al. 1985; Maus and Dimri 1996; Tanaka et al. 1999; Finn and Ravat 2004; Ravat et al. 2007, 2011; Bansal et al. 2011; Nwankwo 2015).

The centroid method is based on examining the shape of isolated magnetic anomalies (Bhattacharyya and Leu 1975, 1977) and studying the statistical properties of magnetic

ensembles by Spector and Grant (1970). Blakely (1995) introduced the theory of power spectral density of total magnetic field and assumed that if the magnetic data set is large enough such that the low-frequency anomalies caused by the bottom of the source are included in the anomaly map, a peak should be recognizable in the spectrum, the central wavenumber of which relates to the depth of the bottom of the sources (Spector and Grant 1970). In this method, estimation of the depth to the centroid (Z_0) is obtained from the logarithm of an azimuthally averaged wavenumber-scaled Fourier amplitude spectrum in the low wavenumber region. Meanwhile, the depths to the top (Z_t) of a magnetic layer which is calculated from the slope of the radially averaged power spectrum of the magnetic anomaly and the bottom depth (Z_b) can be calculated from $Z_b = 2Z_0 - Z_t$ according to Okubo et al. (1985) and Tanaka et al. (1999). Furthermore, the depth resolution in such calculations is restrained to the width of the aeromagnetic window (L), whereby the highest CPD depth estimation is restricted to $L/2$ (Shuey et al. 1977).

In the present study for calculating the Curie point depth, the total intensity aeromagnetic map was divided into forty-nine (49) spectral blocks, each block approximately $137 \times 120 \text{ km}^2$ with 75% overlapping to the adjacent blocks (Fig. 4) and then a generation of radial energy spectrum plots of log energy values versus the wavenumber (k). Two linear segments can be identified for each block, indicating two magnetic source layers in the study area. The red colour line represents the deep source, and the black colour line indicates the external source (Fig. 5). From the two segments, the top (Z_t) and the centroid

Fig. 4 Forty nine overlapping blocks (75%) used for estimating CPD from the TMI map (Curie depth point is located at the centre of the blocks)

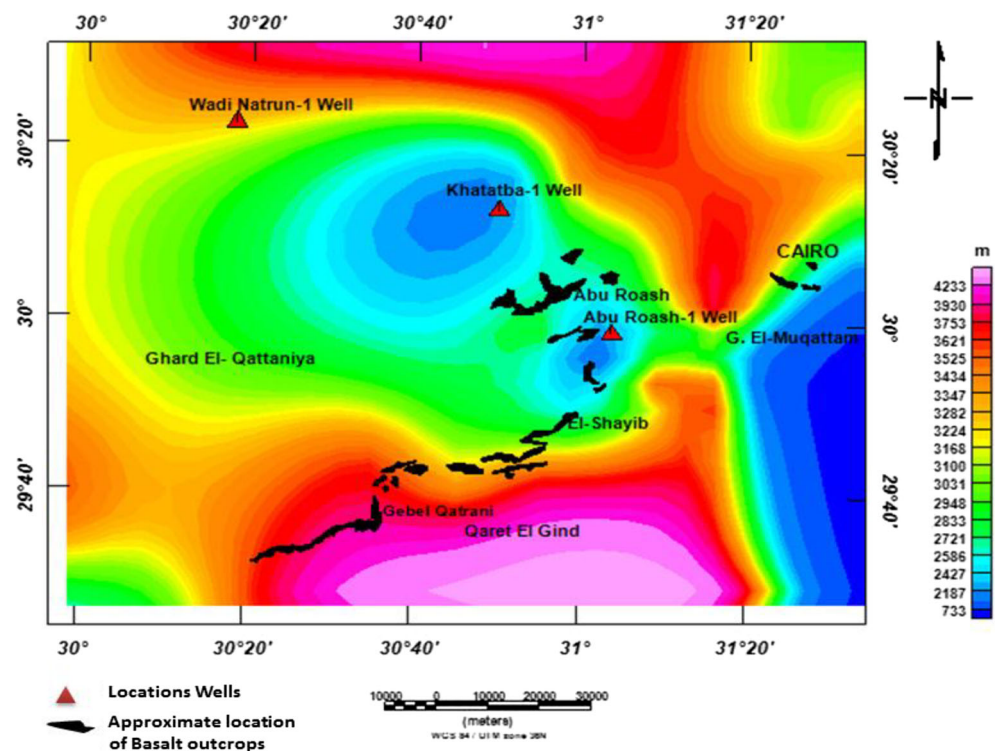
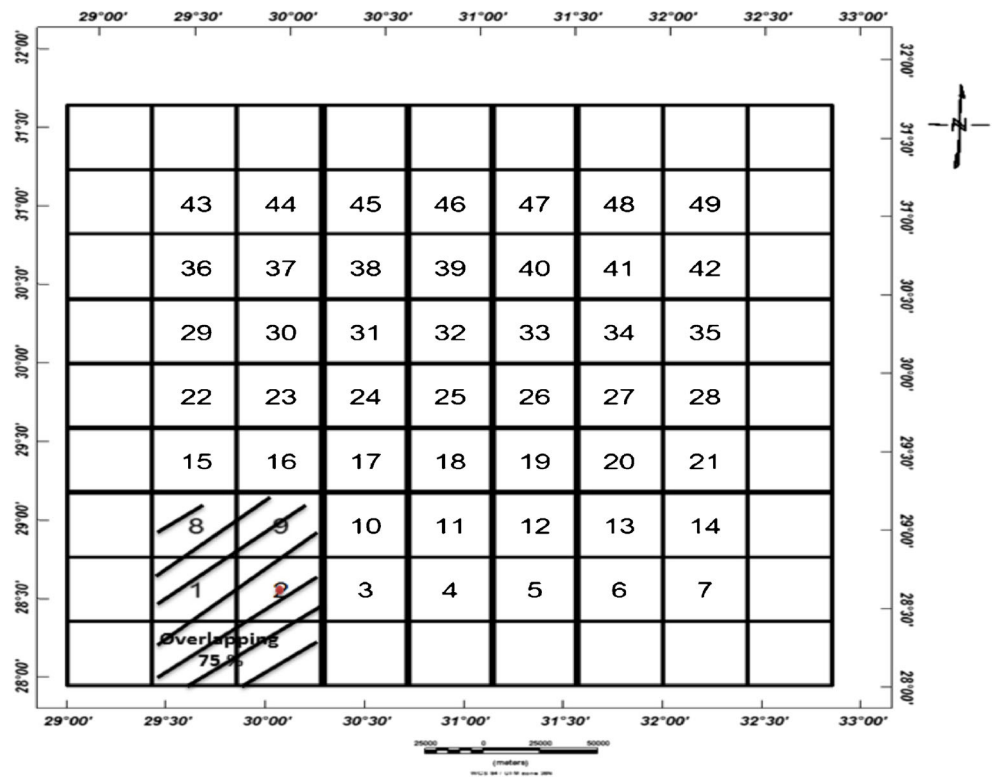


Fig. 5 The radial power spectrum obtained from the TMI map of the study area



(Z_0) depths (the shallow and deep magnetic sources) were calculated by applying the technique of Okubo et al. (1985) and Tanaka et al. (1999). The magnetic source’s bottom depth can be computed as $Z_b = 2 Z_0 - Z_t$, where Z_b is the Curie depth point. This processing was carried out by the Geosoft Oasis Montaj software version 8.3 (2014). The top, centroid, and bottom depth values of each block’s magnetic source are given in Table 1.

Table 1 Lists of top (Z_t), bottom (Z_b), and centroid (Z_0) depth values of the magnetic source obtained for 12 blocks in the study area

Block no.	Z_b (m)	Z_t (m)	Z_0 (m)
23	23120	7904	15512
24	23786	10077	16931
25	21640	8441	15041
26	23780	9086	16433
30	18908	9174	14041
31	25938	8396	17167
32	15717	7755	11736
33	19084	7620	13352
37	20565	11564	16065
38	24464	11122	17793
39	27315	8827	18071
40	26209	9044	17626

The geothermal gradient and heat flow were extracted from the Curie point depth to study the geothermal resources in the study area (Z_b). At 580 °C, the geothermal gradient can be calculated using the equation $dT/dZ = 580 \text{ }^\circ\text{C}/Z_b$ (Tanaka et al. 1999; Stampolidis et al. 2005; Maden 2010). Simultaneously, the heat flow was calculated using the

Table 2 Lists of the derived geothermal gradients and heat flow values from the power spectrum analysis of aeromagnetic map for 12 blocks in the study area. The location of these blocks is shown in Fig. 7

Block no.	Geothermal gradient (C/km)	Heat flow (mW/m ²)
23	25	65
24	24	63
25	27	70
26	24	63
30	31	80
31	22	58
32	37	96
33	30	79
37	28	73
38	24	62
39	21	55
40	22	58

equation: $q = \lambda (dT/dZ) = \lambda (580 \text{ }^\circ\text{C}/Z_b)$, where λ is the coefficient of thermal conductivity.

The study area covers a part of the northern Western Desert; the previously published thermal conductivity measurements for the rocks forming the stratigraphic section in the northern Western Desert carried out by Morgan et al. (1983) were used as reference values. So, the average thermal conductivity was assumed to be $2.6 \text{ W/m}^\circ\text{C}$. The geothermal gradient and heat flow values for each block on the total aeromagnetic intensity map of the area were calculated and shown in Table 2.

Results and discussion

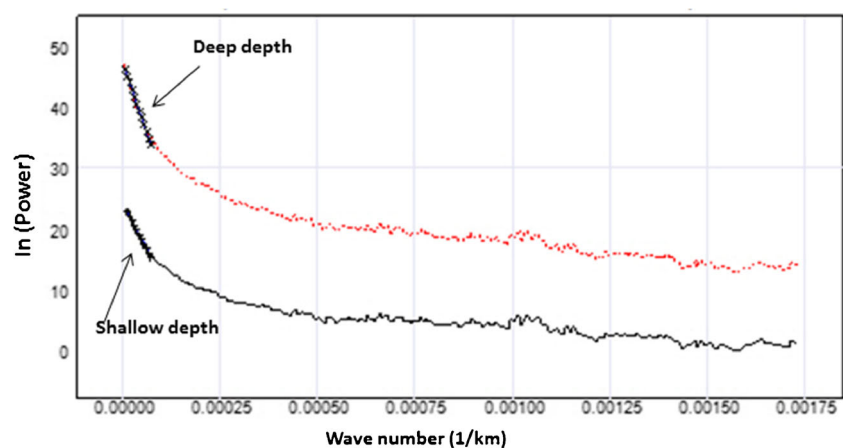
Spectral analysis (SA) and source parameter imaging (SPI) techniques were applied in the quantitative interpretation of the aeromagnetic data. The results of the SPI grid image technique is shown in Fig. 6 and presented as a contour map. The SPI map shows the depth to the basement in the study area ranges from 700 m (shallow magnetic bodies) at the middle and extreme eastern parts of the study area (Khatatba, Abu Raoah, and G. Muqattam) to 4400 m (deep magnetic bodies) at the northern and southern parts (Wadi El Natron and G. Gartani). The SPI technique depth values show good matching with those obtained from the deep wells drilled for oil production in the study area. The sedimentary cover thickness increases northward and southward, corresponding to the El-Gindi basin at the south. El-Gindi basin is one of the promising areas for hydrocarbon occurrences. Meanwhile, uplifts in the shape of anticline are observed in the middle and eastern parts of the study area, corresponding to Abu Roash, El Khatatba, El Shayib, and El Muqattam structure units. The basement depth in the mentioned structure units varies from 700 to 2000 m, below sea level.

On the other hand, the main structural trends in the study area were delineated from the TMI, RTP, and TAD maps which are considered the pathways of basaltic flows. The main trends traced from the TMI map are shown in Fig. 7, from which the major trends are extending in E-W, NE-SW, and NW-SE directions. These trends coincided with the exposed basaltic rocks in the study area, especially at Abu Roash and Gebel Qatrani areas. This coincidence released the fact that basalt in the two areas flowed along the planes of the mentioned structure trends. This fact agrees with what was concluded by Said (1962) and Salem (1976) that the mentioned trends are accompanied by thermal springs and volcanic activity. The depth to basement values were referred to the sea level and the resulting values used in constructing the structure contour map (Fig. 8). The NE-SW and NW-SE fault trends represent the most common structure trends in the basement from the map.

The Curie point depth for the area was calculated from spectral analysis of aeromagnetic data. The results show that the Curie point depth values vary from 14 km in the eastern parts (Cairo, Helwan, El Muqattam, Abu Roash, Haddadin, and Khatatba) and increase to 34 km towards the south-western parts of the area (south Gabal Qatrani), with an average of 20 km (Fig. 9).

In the study area (Fig. 10a,b), the calculated geothermal gradient and heat flow ($2.6 \text{ W/m}^\circ\text{C}$ was used as reference values Morgan et al. 1983) shows that the geothermal gradient values are ranging from 15 to $33 \text{ }^\circ\text{C}/\text{km}$ with an average of approximately $29 \text{ }^\circ\text{C}/\text{km}$. However, the heat flow ranges from 38 to 86 mW/m^2 with an average of approximately 79 mW/m^2 . The geothermal gradient and heat flow values are high at Khatatba and Abu Roash areas, which indicates that the basaltic flows at the mentioned two areas are considered the main source of geothermal resources; moreover, Khatatba and Abu Roash regions are representing geothermal reservoirs that may be used as a non-conventional source of energy. Furthermore, the G. Qatrani region's basaltic flows did not show a tremendous geothermal activity; this may be because the basaltic flows at the mentioned region were cooled and

Fig. 6 SPI depth to the basement surface map in the study area



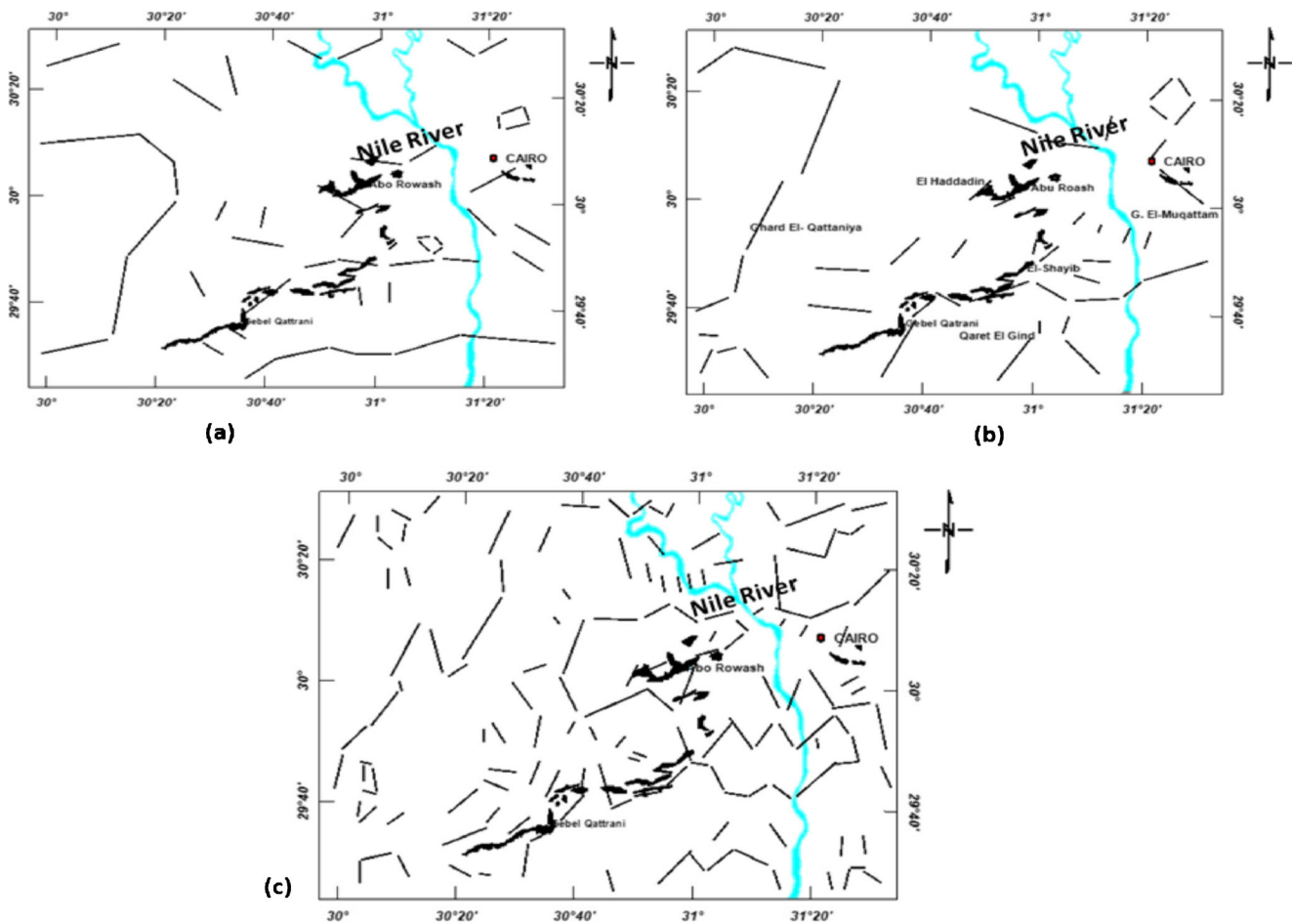


Fig. 7 Magnetic lineaments traced from **a** total magnetic intensity map (TMI), **b** RTP aeromagnetic map, and **c** tilt derivative (TDR) map of the study area

exposed on the surface, lost its temperature, and did not have great geothermal reserve in this region. In Table 3, the results were compared favourably to those previously published by Abdel Zaher et al. (2018); Abdel Zaher (2019), Ebarbary et al. (2018), and Mohamed (2015 and 2019).

Conclusions

The study provides information about the subsurface structures and geothermal activities in the study area by SPI and spectral analysis of aeromagnetic data. SPI results reveal that the predominant structure trends in the study area are extending in E-W, NE-SW, and NW-SE directions. These trends are accompanied by the geothermal and volcanic activity in Western Greater Cairo. Most of the basaltic exposures in the studied area are aligned along with the E-W and NE-SW trends, indicating that the basaltic flows as sheets along the planes of the mentioned trends and the basaltic exposures are rootless. Also, the depth to basement rocks considered the thickness of the sedimentary cover that ranges from 700 to 4400 m.

The Curie point depth was calculated from spectral analysis of aeromagnetic data. The results reveal that the Curie point depth is ranging from 14 km in the eastern parts (Cairo, Helwan, El Mouqattam, Abu Roash, Haddadin, and Khattatba) to 34 km towards the south-western parts of the study area (south of Gabal Qatrani), with an average of 20 km. The geothermal gradient ranges from 15 to 33 °C/km with an average of approximately 29 °C/km. Meanwhile, the heat flow values vary from 38 to 86 mW/m² with an average of approximately 79 mW/m².

These results indicated that the Curie point depth varies inversely with heat flow, where the shallow CPDs, high geothermal gradient, and high heat flow regions, mainly Khattatba and Abu-Roash, are considered geothermal reservoirs and promising regions for a non-congenital energy source. Therefore, the Khattatba and Abu-Roash regions' basaltic flows are considered the main geothermal source but are not at the G. Qatrani region. On the other hand, the thickness of the sedimentary cover is great at the southern parts of the study area, forming an El-Gendi basin that indicates hydrocarbon occurrences. This basin has drilling activities for hydrocarbon production nowadays.

Fig. 8 The predominant major structure trends in the study area, as interpreted from the depth to the basement map

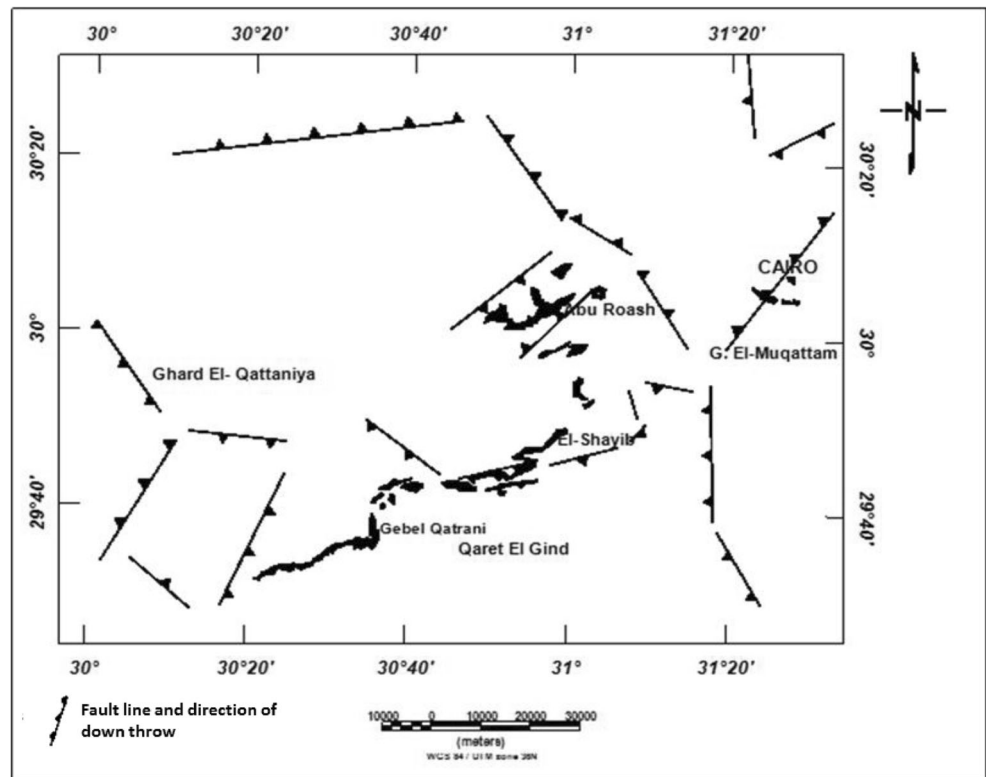
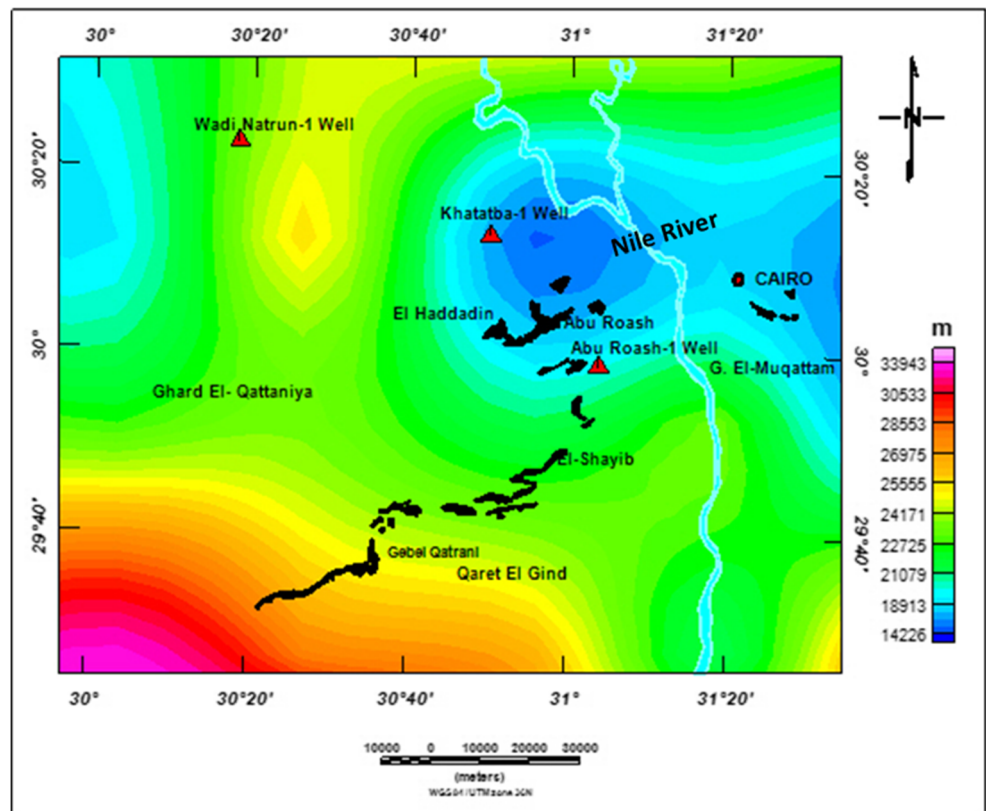


Fig. 9 Map of the Curie depths of the study area



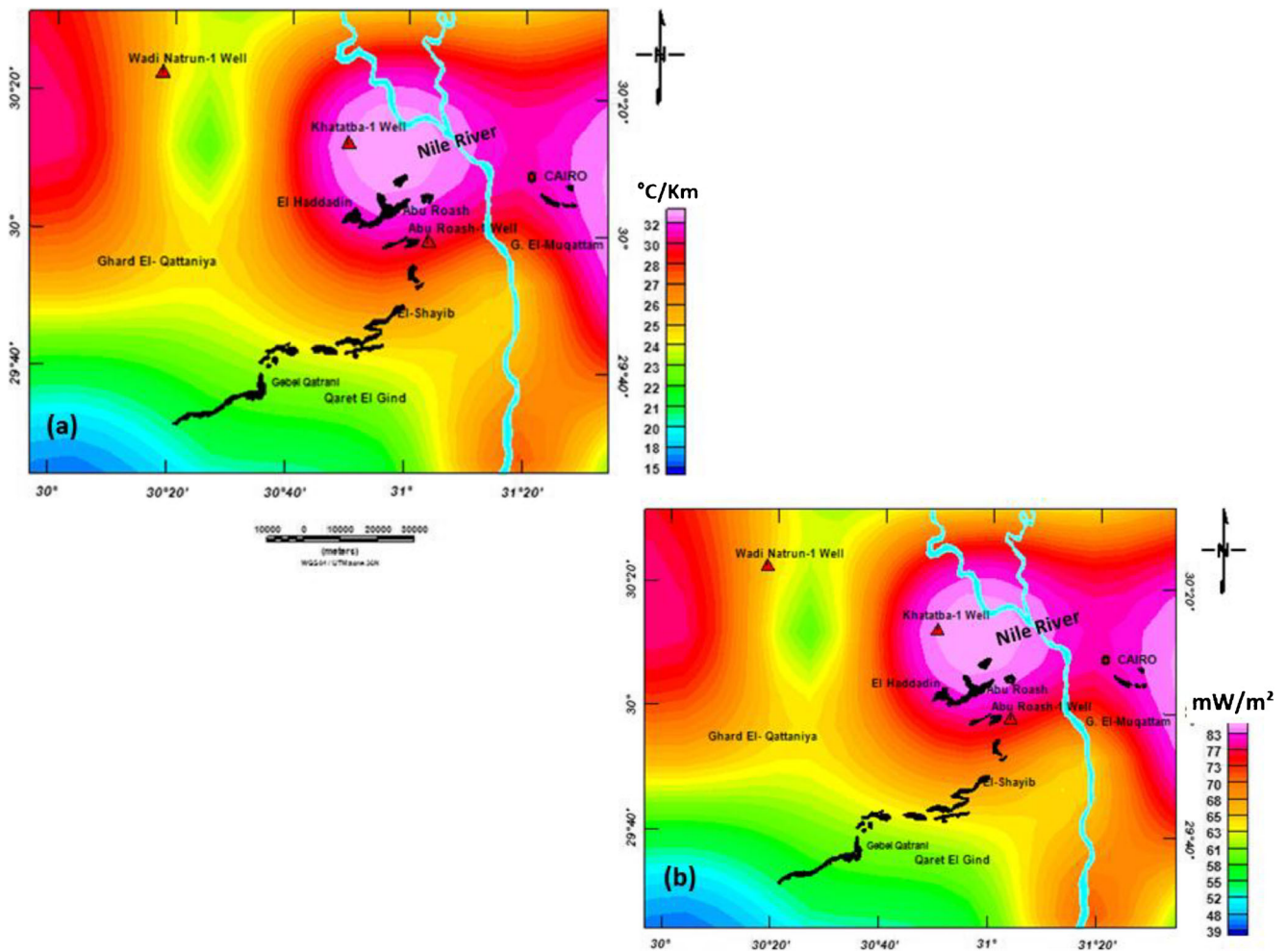


Fig. 10 a Geothermal gradient map. b heat flow map of the study area using an average thermal conductivity of 2.6 W/m°C

Table 3 Comparison between results the geothermal potentiality of the current study and the published from all Egypt

Curie Point Depth (CPD)	Geothermal gradient (G.G)	Heat flow	References	The area
from 14 km to 34km, with an average of 20 km	From 15 °C/km to 33 °C/km with an average of approximately 29 °C/km.	From 38 to 86 mW/m ² with an average of approximately 79 mW/m ² .	In the current paper	The current area (West Cairo area, Egypt)
From 8.9 to 35km with an average value of 20km	From 17.6 to 75 °C/km. The average value is about 31 °C/km which is closer to the world average (30 °C/km).	From 26.9 to about 187mWm ² with an average of about 78.5mW/m ² .	Abdel Zaher et al. (2018)	All Egypt
From 8.6 to 35.7 km	From 16.3 to 67.4 °C/km.	From 47.1 to about 195.5 mWm ² with an average of about 78.5mW/m ² .	Elbarbary et al. (2018)	All Egypt
	from 20 C°/km to 40°C/km.		Mohamed et al. (2015)	Northern Western Desert of Egypt
From 21 to 28km	From 21 to 27 °C/km.	From 49 to about 64mW/m ²	Abdel Zaher et al. (2018)	Siwa Oasis, Western Desert
From 17 km to 29 km, with an average of 25 km	From 20 to 35°C/km and an average of approximately 30 °C/km.	from 52 to 90 mW/m ² with an average of approximately 66mW/m ² .	Mohamed et al. (2019)	Bahariya Oasis, Western Desert
From 18 km to 26 km	From 18.39 °C/km to 36 °C/km and an average of around 26 °C/km,	53 to 104 mW/m ² with an average of approximately 74mW/m ²	Abdel Zaher et al. (2019)	Farafra Oasis, Western Desert

Declarations

Conflict of interest The author(s) declare that they have no competing interests.

References

- Aadland AJ, Hassan AA (1972) Hydrocarbon potential of the Abu Gharadig basin in the Western Desert, Egypt. 8th Arab Petrol. Cong., Algiers, No. 81(B-3)
- Abdel Monem AA, Heikal MA (1981) Major element composition, magma type and tectonic environment of the Mesozoic to Recent basalts, Egypt. Bull. Fac. Earth Sci., King Abdul Aziz Uni., Jeddah 4: 121–148
- Abdel Zaher M (2019) Exploration of geothermal resources in Farafra Oasis, Western Desert, Egypt, 44th Workshop on Geothermal Reservoir Engineering Stanford University, Stanford, California, SGP-TR-214
- Abdel Zaher M, Elbarbary S, El-Shahat A, Mesbah H, Embaby A (2018) Geothermal resources in Egypt integrated with GIS-based analysis. J Volcanol Geotherm Res:0377–0273. <https://doi.org/10.1016/j.jvolgeores>
- Aboud, E., Salem, A., S., Mekki, M., (2011): Curie depth map for Sinai Peninsula, Egypt deduced from the analysis of magnetic data, Journal of Tectonophysics 506(1):46–54, doi: <https://doi.org/10.1016/j.tecto.2011.04.01>
- Abu El-Rus MA, Rooney TO (2017) Tertiary volcanic activity of the middle Egypt: a probe for asthenosphere-lithosphere interaction in northeast Africa. Chem Geol 455:282–303
- Abu El-Rus MA, Chazot G, Vannucci R, Paquette JL, (2018) Tracing the HIMU component within Pan-African lithosphere beneath northeast Africa: evidence from Late Cretaceous Natash alkaline volcanics, Egypt. Lithos 300–301 136–153
- Amer K, Samuel MD, Saleeb- Roufael GS (1982) Petrography and petrochemistry of the subsurface basalts of Mit Ghamr and Abu Hammad wells. Egypt J Geol 26:83–94
- Aydin I, Oksum E (2010) Exponential approach to estimate the Curie-temperature depth. J Geophys Eng 7:113–125
- Baldrige WS, Eyal Y, Bartov Y, Steinitz G, Eyal M (1991) Miocene magmatism of Sinai related to the opening of the Red Sea. Tectonophysics 197:181–201
- Bansal AR, Gabriel G, Dimri VP, Krawczyk CM (2011) Estimation of the depth to the bottom of magnetic sources by a modified centroid method for fractal distribution of sources: an application to aeromagnetic data in Germany. Geophysics 76(3):L11–L22
- Bansal AR, Anand SP, Rajaram M, Rao VK, Dimri VP (2013) Depth to the bottom of magnetic sources (DBMS) from aeromagnetic data of central India using modified centroid method for fractal distribution of sources. Tectonophysics 603:155–161
- Bayoumi, A.I., Sabri, A., (1971): A contribution to magnetic anomalies in the Quatrani – El Natrun area. Bull. Fac. Sci., Cairo Univ. 40:165–173
- Bhattacharyya BK, Leu LK (1975) Analysis of magnetic anomalies over Yellowstone National Park: mapping of Curie point isothermal surface for geothermal reconnaissance. J Geophys Res 80(32):4461–4465
- Bhattacharyya BK, Leu LK (1977) Spectral analysis of gravity and magnetic anomalies due to rectangular prismatic bodies. Geophysics 42: 41–50
- Blakely RJ (1995) Potential theory in gravity and magnetic applications, Cambridge Univ. Press, Cambridge
- Bowen BE, Vondra CF (1974) Paleoenvironmental interpretations of the Oligocene Gabal el Qatrani Formation, Fayum Depression, Egypt: Annals of the Geological Survey of Egypt, v. 4, p 115–138
- Chapman DS, Furlong KP (1992) Thermal state of continental lower crust, in: Continental lower crust, edited by: Fountain, D.M., Arculus, R., and Kay, R. W., Elsevier Science, Amsterdam, 179–199.
- Dogan G, Saibi H, Gabr A, Bloushi K, Alkaabi A (2017) Curie point depth from spectral analysis of magnetic data for geothermal reconnaissance in Mubazarah Area – Al Ain –United Arab Emirates, 1st Middle East Geoscience Student Conference 2017. UAEU, Al-Ain, 26th February to 1st March 2017
- Elbarbary S, Abdel Zaher M, Mesbah H, El-Shahat A, Embaby A (2018) Curie point depth, heat flow and geothermal gradient maps of Egypt deduced from aeromagnetic data. J Renew Sustain Energy Rev 91: 620–629
- Endress C, Furman T, Abu El-Rus MA, Hanan BB (2011) Geochemistry of 24 Ma basalts from NE Egypt: source components and fractionation history. In: Van Hinsbergen DJJ, Buitter SJH, Torsvik TH, Gaina C, Webb SJ (eds) The formation and evolution of Africa: a synopsis of 3.8 Ga of Earth history, vol 357. Geological Society, London, Special Publications, pp 265–283
- Finn CA, Ravat D (2004) Magnetic depth estimates and their potential for constraining crustal composition and heat flow in Antarctica, EOS T. Am. Geophys. Un., 85, Fall meeting Suppl., Abstract T11A-1236
- Gay SP Jr. (1972) Fundamental characteristics of aeromagnetic lineaments, their geologic significance, and their significant to geology. The New Basement Tectonics. American Stereo map Company, Salt Lake City, Utah p 94
- Getech (1992) The African magnetic mapping project—commercial report (unpublished)
- Gingerich PD (1992) Marine mammals (Cetacea and Sirenia) from the Eocene of Gebel Mokattam and Fayum, Egypt: stratigraphy, age and paleoenvironments. University of Michigan Papers on Paleontology 30:1–84
- Green CM, Barritt SD, Fairhead JD, Misener DJ (1992) The African magnetic mapping project. Extended abstract, EAEG 54th Meeting and Technical Exhibition, Paris
- Hochstein MP (1990) Classification and assessment of geothermal resources. In: Dickson MH, Fanelli M (eds) Small geothermal resources: a guide to development and utilization. UNITAR, New York, pp 31–57
- Hsieh HH, Chen CH, Lin PY, Yen HY (2014) Curie point depth from spectral analysis of magnetic data in Taiwan. J Asian Earth Sci 90: 26–33. <https://doi.org/10.1016/j.jseaes.2014.04.007>
- Kamba AH, Ahmed SK (2017) Depth to basement determination using source parameter imaging (SPI) of aeromagnetic data: an application to Lower Sokoto Basin, Northwest, Nigeria. International Journal of Modern Applied Physics 7(1):1–10
- Komolafe AA (2010) Investigations into the tectonic lineaments and thermal structure of Lake Magadi, Southern Kenya Rift using integrated geophysical methods. Unpublished M.Sc. Thesis. International Institute of Geo-Information Science and Earth Observation, Enschede, The Netherlands
- Lucassen F, Franz G, Romer RL, Pudlo D, Dulski P (2008) Nd, Pb, and Sr isotope composition of Late Mesozoic to Quaternary intra-plate magmatism in NE-Africa (Sudan, Egypt): high-*f* signatures from the mantle lithosphere. Contrib Mineral Petrol 156:765–784
- Maden N (2010) Curie-point depth from spectral analysis of magnetic data in Erciyes stratovolcano (Central TURKEY). Pure Appl Geophys 167:349–358
- Maus S, Dimri VP (1996) Depth estimation from the scaling power spectrum of potential fields. Geophys J Int 124:113–120
- Miller HG, Singh V (1994) Potential field tilt—a new concept for location of potential sources. Appl Geophys 32:213–217

- Moghazi A (2003) Geochemistry of a tertiary continental basalt suite, Red Sea coastal plain, Egypt: petrogenesis and characteristics of the mantle source region. *Geol.Mag.* 140:11–24
- Mohamed HS (2021) Subsurface structures and conceptual hydrothermal model of the area lying between Quseir and Safaga area, Red Sea Coast, Egypt. *Arab J Geosci* 14:49. <https://doi.org/10.1007/s12517-020-06294-7>
- Mohamed HS, Abdel Zaher M Subsurface structural features of the basement complex and geothermal resources using aeromagnetic data in the Bahariya Oasis, Western Desert, Egypt. 2019, *J Pure Appl Geophys* 177(2020):2791–2802. <https://doi.org/10.1007/s00024-019-02369-z>
- Mohamed HS, Abdel Zaher M, Senosy MM, Saibi H, El Nouby M, Fairhead D (2015) Correlation of aerogravity and BHT data to develop a geothermal gradient map of the Northern Western Desert of Egypt using an artificial neural network. *J Pure Appl Geophys* 172(6):1585–1597
- Morgan P, Boulos FK, Swanberg CA (1983) Regional geothermal exploration in Egypt. *Geophys Prospect* 31:361–376
- Nabighian MN (1972) The analytic signal of two dimensional magnetic bodies with polygonal cross-section: its properties and use for automated anomaly interpretation. *Geophysics* 37(3):507–517
- Norton P (1967) Rock stratigraphic nomenclature of the Western Desert. Internal Report of GPC, Cairo, Egypt, 557 p
- Nur A, Ofoegbu CO, Onuoha KM (1999) Estimation of depth to the Curie point isotherm in the Upper Benue Trough, Nigeria. *J Min Geol* 35(1):53–60
- Nwankwo LI (2015) Estimation of depths to the bottom of magnetic sources and ensuing geothermal parameters from aeromagnetic data of Upper Sokoto Basin Nigeria. *Geothermics* 54:76–81
- Nwankwo LI, Shehu AT (2015) Evaluation of Curie-point depths, geothermal gradients and near-surface heat flow from high resolution aeromagnetic (HRAM) data of the entire Sokoto Basin, Nigeria. *J Volcanol Geotherm Res* 305:45–55
- Oasis Montaj Programs (2014) Geosoft mapping and processing system: Version 8.3. (HJ), Inc Suit 500, Richmond St. West Toronto, ON Canada N5S1V6
- Okubo Y, Graf RJ, Hansen RO, Ogawa K, Tsu H (1985) Curie point depths of the island of Kyushu and surrounding areas, Japan. *Geophysics* 50:481–494
- Raj K, Bansal AR, Betts PG, Ravat D (2021) Re-assessment of the depth to the base of magnetic sources (DBMS) in Australia from aeromagnetic data using the defractal method. *Geophys J Int* 225(1):530–547. <https://doi.org/10.1093/gji/ggaa601>
- Ravat D, Pignatelli A, Nicolosi I, Chiappini M (2007) A study of spectral methods of estimating the depth to the bottom of magnetic sources from near-surface magnetic anomaly data. *Geophys J Int* 169:421–434
- Ravat D, Salem A, Abdelaziz AMS, Elawadi E, Morgan P (2011) Probing magnetic bottom and crustal temperature variations along the Red Sea margin of Egypt. *Tectonophysics* 510:337–344
- Refai E, Riad S, Tealab A, (1973) The main tectonic trends of west Cairo area, Egypt. *Egypt. Bull.*, no.2
- Rittmann A (1954) Remarks on the eruptive mechanism of the Tertiary volcanoes of Egypt. *Bull Volcanol* 15:109–117
- Ross HE, Blakely RJ, Zoback MD (2006) Testing the use of aeromagnetic data for the determination of Curie depth in California. *Geophysics* 71(5):L51–L59
- Saibi H, Aboud E, Azizi M (2015a) Curie point depth map for Western Afghanistan deduced from the analysis of aeromagnetic data: World Geothermal Congress, 19-24 April 2015 Australia—New Zealand
- Saibi H, Aboud E, Gottsmann J (2015b) Curie point depth from spectral analysis of aeromagnetic data for geothermal reconnaissance in Afghanistan. *J Afr Earth Sci* 111:92–99
- Said R (1962) The geology of Egypt. Elsevier Publishing Company, Amsterdam, New York
- Said R (1981) The geological evolution of the River Nile. Springer, 151 pp
- Said R (1990) The geology of Egypt. A. A. Balkema Publishers, Rotterdam, Netherlands 734 pp.
- Salem R (1976) Evolution of Eocene-Miocene sedimentation patterns in parts of northern Egypt. *Am Assoc Pet Geol Bull* 60:34–64
- Shuey RT, Schellinger DK, Tripp AC, Alley LB (1977) Curie depth determination from aeromagnetic spectra. *Geophys J R Astron Soc* 50:75–101
- Spector A, Grant FS (1970) Statistical models for interpreting aeromagnetic data. *Geophysics* 35:293–302
- Stampolidis A, Kane I, Tsokas GN, Tsourlos P (2005) Curie point depths of Survey Department. Ministry of Public Works, Egypt, 84 p
- Swedan AH (1991) A note on the geology of greater Cairo area. *Annals of the Geological Survey of Egypt*:239–251
- Tanaka A, Okubo Y, Matsubayashi O (1999) Curie point depth based on spectrum analysis of the magnetic anomaly data in East and Southeast Asia. *Tectonophysics* 306:461–470
- Thurston JB, Smith RS (1997) Automatic conversion of magnetic data to depth, dip, and susceptibility contrast using the SPITM method. *Geophysics* 62(3):807–813
- Verduzco B, Fairhead JD, Green CM, MacKenzie C (2004) New insights into magnetic derivatives for structural mapping. *Lead Edge* 23: 116–119
- Williams GA, Small JO (1984) A study of the Oligo-Miocene basalts in the Western Desert. *Proc. 7th petrol. Explor. Seminar, EGPC, Cairo*: 252-268